LARGE EDDY SIMULATION OF SEPARATED FLOW OVER A BLUFF PLATE

Anotai Suksangpanomrung, Ned Djilali
Department of Mechanical Engineering, University of Victoria
British Columbia, V8W 3P6, Canada

Philippe Moinat
CERFACS, 31057 Toulouse
Cedex 1, France

ABSTRACT

The turbulent separated-reattaching flow over a bluff plate is investigated using the large-eddy simulation approach. The simulations were performed at a Reynolds number (Ud/ν) of 50,000 and a blockage ratio of 5.7%. Three subgrid-scale models were used: structure function, selective structure function and Smagorinsky models. The performance of these models was examined by comparing the mean flow statistics and the dynamics of the flow with experimental observations. With both structure-function and Smagorinsky models, the breakup and three dimensionalization of the separated shear layer are delayed. The dynamics of the reattaching flow is altered by the persistence of small-scale structures in the Smagorinsky model simulation, while excessive subgrid-scale dissipation is evident in the structure-function simulation. Both models yield deficient mean flow structures and turbulence statistics. The selective version of the structure function model, which allows a localization of the subgrid-scale contribution, produces separated shear layer instabilities, dynamical patterns, and structure which are physically consistent with flow visualization. The mean flow and turbulent statistics obtained with the model are also found to be in excellent agreement with measurements. A preliminary wavelet analysis of the simulations reveals the persistence of scales associated with shear-layer flapping and the intermittent nature of the pseudo-periodic shedding of vortices in the reattachment region.

INTRODUCTION

Flows with large regions of separation occur in a variety of environmental and engineering applications. Large-scale unsteadiness, complex turbulent structure, curvature effects and large pressure gradients characterize these flows. Many of these features have been challenging to predict using Reynolds-Averaged turbulence models. In this paper, we investigate the unsteady separated-reattaching flow around a bluff rectangular plate using the large-eddy simulation (LES) technique. This "benchmark" bluff plate geometry, which is relevant to heat exchanger applications and is shown in Fig. 1, simplifies considerably the study of separated-reattaching flows: the location of separation is fixed; the shear layer at separation is thin; and the upstream boundary conditions are simple and well defined. This eliminates the need for a prohibitively large upstream computational domain to allow the development of upstream profiles with the correct turbulence characteristics. Also , for a sufficiently long plate, the separated shear layers on the top and bottom of the plate reattach to the surface and do not interact.

The mean flow characteristics and large scale unsteadiness aspects of turbulent flow around bluff rectangular plate have been the subject of a number of experimental studies at high Reynolds numbers ($\gtrsim$ 20,000) (e.g., Cherry *et al.*, 1983; Kiya *et al.*, 1983; Djilali and Gartshore, 1991a; Saathoff and Melbourne, 1997). All studies report a characteristic low frequency flapping of the separated shear layer as well as pseudo-periodic vortex shedding from the separation bubble. A strong dependence on free stream turbulence has been reported (Hillier and Cherry, 1981; Saathoff and Melbourne, 1997), with for instance reduction of up to 50% in the mean reattachment length $\bar{X}_r$ and significant changes in the dynamics of the flow and spanwise length scales. The direct numerical simulation of Tafti and Vanka (1991) have reproduced many of the large-scale characteristics observed at higher Reynolds numbers, but were confined to a Reynolds number of 1000.

Reynolds-averaged Navier-Stokes (RANS) of the high Reynolds number turbulent flow (Djilali *et al.*, 1991b)

have provided an adequate representation of the mean flow characteristic within the separation bubble. However ad-hoc modifications of the turbulence model were required, and, even then, a marked deterioration of the predictions in the recovery region was noted. Furthermore, such RANS computations cannot provide information on the complex dynamics of the flow and on the large-scale unsteadiness that dominate turbulent transport. To investigate these features and provide a detailed description of the turbulent transport description, large-eddy simulations undertaken at a Reynolds number of 50,000 are presented in this paper.

COMPUTATIONAL METHODS

Mathematics Model

The governing equations for the large scale (resolved) motion can be obtained by applying a spatial filter (indicated by an overbar) to both the continuity and the Navier-Stokes equations, with the result (Ferziger, 1993; Lesieur and Métais O., 1996);

$$\frac{\partial \bar{u}_i}{\partial x_i} = 0 \tag{1}$$

$$\frac{\partial \bar{u}_i}{\partial t} + \frac{\partial \bar{u}_i \bar{u}_j}{\partial x_j} = -\frac{1}{\rho}\frac{\partial \bar{p}}{\partial x_i} + \nu \frac{\partial^2 \bar{u}_i}{\partial x_j^2} + \frac{\partial T_{ij}}{\partial x_j} \tag{2}$$

where the subgrid-scale tensor $T_{ij} = \bar{u}_i\bar{u}_j - \overline{u_i u_j}$, which represent the lumped effect of the subgrid-scales on the resolved scales, is modelled using an eddy-viscosity assumption;

$$T_{ij} = \nu_t\left(\frac{\partial \bar{u}_i}{\partial x_j} + \frac{\partial \bar{u}_j}{\partial x_i}\right) + \frac{1}{3}T_{kk}\delta_{ij} \tag{3}$$

In this study, the eddy viscosity ν_t is evaluated using three subgrid-scale (SGS) models: the structure function (SF), selective structure function (SSF) and Smagorinsky models (SM). In the structure function model, the eddy-viscosity is evaluated according to (Lesieur and Métais O., 1996);

$$\nu_t(x, \Delta_c, t) = 0.063\Delta_c\sqrt{\bar{F}_2(\mathbf{x}, \Delta_c, t)} \tag{4}$$

where Δ_c is the mean mesh size, and $\bar{F}_2$ is the second order structure function of the resolved velocity field for a radius Δ_c;

$$\bar{F}_2(\mathbf{x}, \Delta_c, t) = \langle \|\bar{\mathbf{u}}(\mathbf{x}+\mathbf{r}, t) - \bar{\mathbf{u}}(\mathbf{x}, t)\|^2 \rangle_{\|\mathbf{r}\|=\Delta_c} \tag{5}$$

In the selective version of the structure function model, better localization of the small-scale turbulence is achieved by switching off the eddy-viscosity when the flow is not sufficiently three-dimensional. The measure of three-dimensionality used is the angle between the local vorticity vector and the average vorticity over the neighbouring points. The Smagorinsky model is implemented with a damping function (see Kogaki *et al.*, 1997);

$$\nu_t(x, \Delta_c, t) = (0.13D\Delta_c)^2(2\bar{S}_{ij}\bar{S}_{ij})^{1/2} \tag{6}$$

where D is the Damping function, $D = 1 - e^{\frac{-y^+}{A}}$, and $\bar{S}_{ij}$ is the strain rate, $\bar{S}_{ij} = \frac{1}{2}(\frac{\partial \bar{U}_i}{\partial x_j} \frac{\partial \bar{U}_j}{\partial x_i})$.

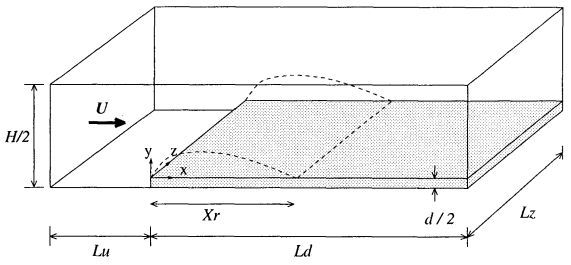

Figure 1: Computational domain, $Lu = 4d, Ld = 12d, Lz = 5.2d, d/H = 0.057$

Numerical Method

A staggered grid, finite volume method was used. Mixed discretization is adopted in the computational domain, i.e.: central differencing (CD) is used downstream of the leading edge of the plate to ensure that the simulations in the zone of interest are free from numerical dissipation; and a quadratic upwind scheme (QUICK) is used in the region upstream of the plate to avoid the generation of spurious oscillations in the high gradient region immediately upstream of the leading corner of the plate. This procedure was adopted following a preliminary investigation (Suksangpanomrung *et al.*, 1997) in which small perturbations arising from the use of the unbounded CD scheme in the upstream region were found to have an effect similar to increased free-stream turbulence.

A 3rd order Runge-Kutta algorithm is used for time integration in conjunction with a classical correction method at each sub-step. The continuity equation (1) and the pressure gradient term in the momentum equation (2) are treated implicitly, while the convective and diffusive terms are treated explicitly. The linear system for pressure is solved by an efficient conjugate gradient method with preconditioning.

Computational domain and boundary conditions

A schematic of the flow domain is shown in Fig. 1. The simulations were performed at a Reynolds number (Ud/ν) of $5\text{x}10^4$ and for a blockage ratio, d/H, of 5.7%; this corresponds to the experimental conditions used by Djilali and Gartshore (1991a). A computational grid of N_x x N_y x N_z = 108 x 61 x 27 was used, with non-uniform distributions in the x and y directions. The extent of the domain Lz in the periodic (spanwise) direction is over twice the spanwise correlation length obtained by Saathoff and Melbourne (1997).

At the inlet and outlet, uniform flow and advective conditions are imposed. Symmetry is imposed along the lower boundary upstream of the plate; the surface of the plate and the upper boundary are no-slip walls. An approximate wall function is used on all solid boundaries. Though known to be inadequate, such a treatment is currently unavoidable at high Reynolds numbers.

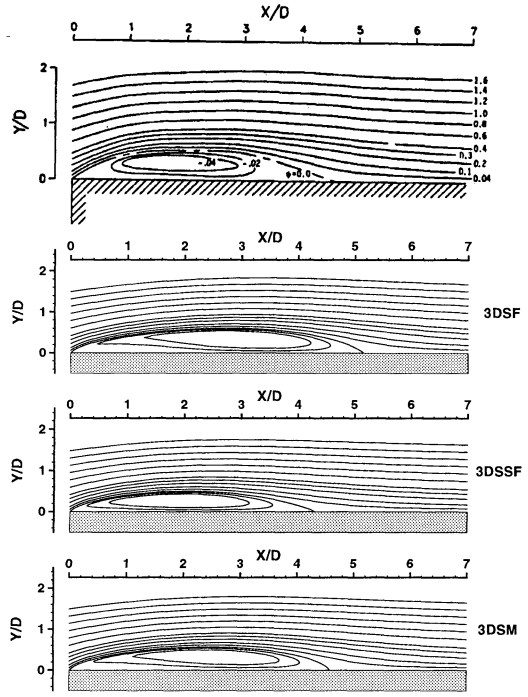

Figure 2: Mean streamline patterns

RESULTS AND DISCUSSIONS

Time-Averaged Characteristics

The time mean reattachment lengths obtained with the three SGS models are given in Table 1, together with the sampling time for each model. The time step is floated and adjusted with the CFL condition, but is of the order of $0.006tU/d$ for 3DSF and 3DSM and $0.003tU/d$ for 3DSSF. Simulations over an initial "start-up" period of about $50tU/d$ were discarded to allow the passage of initial transients. Following this, all simulations were integrated over $400tU/d$; i.e. about 35 "residence" times in the region downstream of separation. The spanwise and time-averaged streamline patterns from all three simulations are compared to experiments in Fig. 2. Although 3DSM provides the best prediction of $\bar{X}_r$, the mean flow pattern of 3DSSF is more physical, with both shape and location of the centre of recirculating flow vortex comparing better with experiments.

TABLE 1. MEAN REATTACHMENT LENGTH AND SAMPLING TIME FOR THREE SIMULATION [1]

Run	SGS models	Sampling times (tU/d)	$\bar{X}_r/d$
3DSF	SF	400	5.14
3DSSF	SSF	400	4.30
3DSM	SM	400	4.57
Expt	—	—	4.7± 0.1

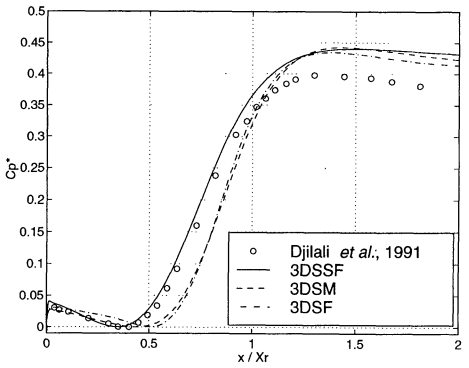

Figure 3: Mean reduced surface pressure coefficient distributions

The computed mean pressure distributions along the upper surface of the plate are compared with measurements in Fig. 3. The experimental trend is reproduced reasonably well by all three simulations, but 3DSSM provides better agreement with the location of the minimum at x $\approx 0.4\ \bar{X}_r$, and the recovery rate afterwards. The recovery process is completed by x $\approx 1.3\bar{X}_r$; a 10% or so overestimate of the pressure coefficient is observed thereafter. This is probably due, in part, to the "ventilation" from the base of the plate likely to occur in the experimental flow as a result of the finite plate length. In the flow region x $\gtrsim 1.3\bar{X}_r$ we note the under-predicted pressure gradient in 3DSSF. The flow in this region is dominated by the redeveloping boundary layer and this feature possibly indicates inadequate wall treatment.

Figure 4 compares the mean streamwise velocity profiles at several stations along the plate with pulsed-wire measurements. The 3DSSF profiles are in very good agreement with measurements at all stations, but both 3DSF and 3DSM predict a broader backflow profile and underestimate the peak backflow velocity over the first half of the separation bubble. This results in the pinched streamline patterns in Fig. 2. Further downstream, all three simulations result in similar profiles. In the recov-

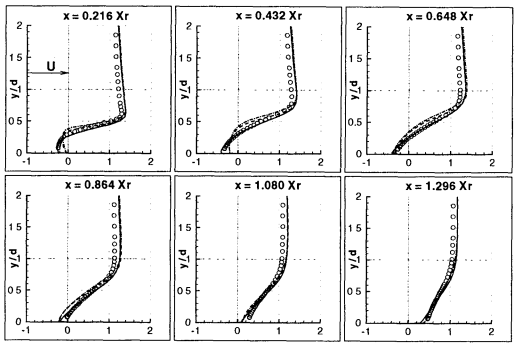

Figure 4: Mean streamwise velocity profiles: Experimental, circle; 3DSSF, solid line; 3DSM, dashed line; 3DSF, dot-dashed line

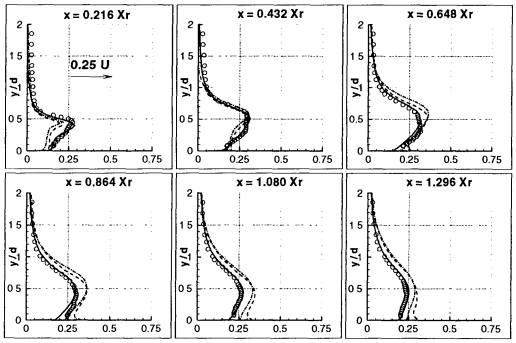

Figure 5: Longitudinal turbulent intensity ($< u' > /U$) profiles: Experimental, circle; 3DSSF, solid line; 3DSM, dashed line; 3DSF, dot-dashed line

ery region, we note that the LES simulations do not suffer from the commonly observed velocity defect obtained with RANS computations (Djilali *et al.*, 1991b).

The turbulent intensity profiles, including both resolved and subgrid scale contributions, are presented in Fig. 5. The 3DSSF simulation yields remarkably good agreement with experimental data throughout. The cusp near the leading edge is well reproduced; the correct evolution of the maximum intensities with x is obtained, and a maximum values of $< u' >$ of around $0.3U$ is attained in the last third of the mean separation bubble in agreement with measurements.

The 3DSF and 3DSM profiles, on the other hand, have noticeable deficiencies. The intensities are underestimated on the low side of the separated shear layer for $x/\bar{X}_r < 0.4$, and are overestimated on the upper high velocity side of the shear layer for $x/\bar{X}_r > 0.5$. In 3DSM, where wall damping is used, we note the appearance of a near-wall peak after $x/\bar{X}_r > 0.6$. Available measurements do not resolve the near-wall region, but the appearance of a near-wall peak in the recovery region, $x/\bar{X}_r > 1.2$, is not unrealistic; such a feature was reported in the highly resolve DNS of the low Re flow over a backward-facing step of Le *et al.* (1998).

Profiles not presented here, show that the contribution of the subgrid-scales to the tangential Reynolds stress

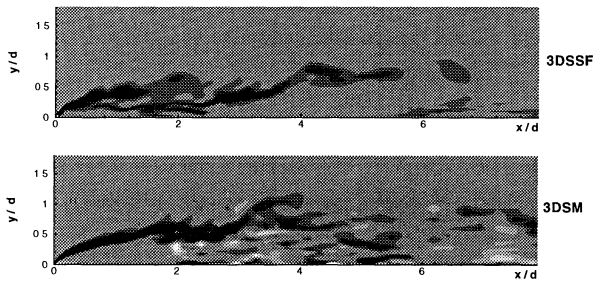

Figure 6: Instantaneous spanwise vorticity contour in x-y plane at z = $2.6d$: 10 contours from -$10U/d$ to $5U/d$

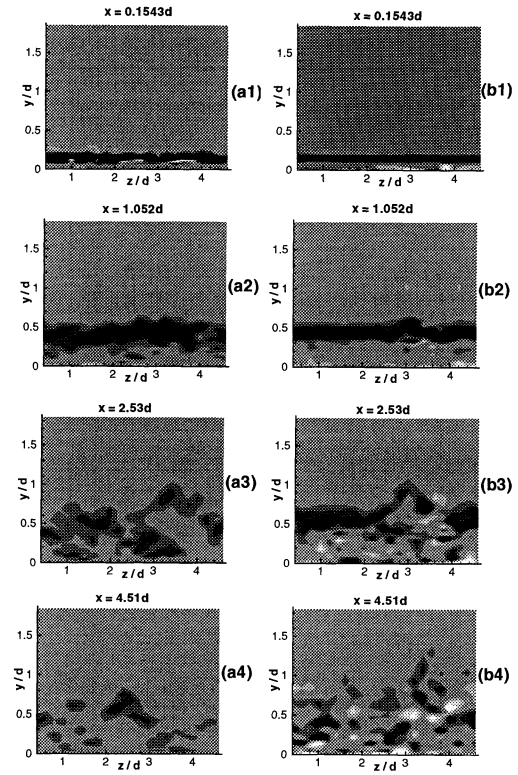

Figure 7: Instantaneous spanwise vorticity contours in y-z plane:(a1, a2, a3 and a4) 3DSSF; (b1, b2, b3 and b4) 3DSM

components for 3DSSF is generally small near separation and reaches about 25% for $< u'^2 >$ in the reattachment region. The subgrid-scale contribution to $- < u'v' >$ is about 20-25% in both separation and reattachment regions. In 3DSF, the contribution of the model to the normal stresses is larger than that to the shear stresses, whereas in the Smagorinsky model, the subgrid scale contribution is minimal ($\sim$ 2%). The dissipation provided by this model is, in the mean, very small and confined to the early part of the separated shear layer. It should be noted that the constant used here is that recommended by Kogaki *et al.* (1997) for separated flows and is lower than the "standard" value used in boundary layer simulations. Both structure function models produce larger subgrid-scale dissipation in the reattachment zone, but much higher levels are obtained with 3DSF. Therefore, we expect the latter to have a much stronger influence on the dynamics of the flow in the reattachment zone.

Flow Structures

Instantaneous spanwise vorticity fields from the selective structure function (3DSSF) and the Smagorinsky model (3DSM) simulations are shown in Fig. 6. In the case of 3DSM, no significant fluctuations are detected in the separated shear layer till $x/d \approx 1.8$, whereas

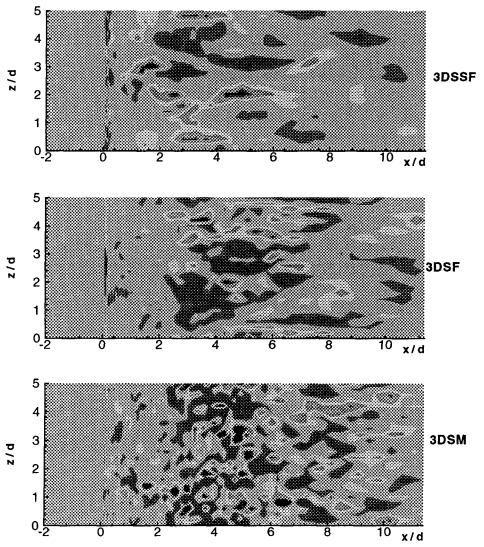

Figure 8: Instantaneous streamwise vorticity contours in x-z plane at y = $0.120d$: 8 contours from -$5U/d$ to $2U/d$

instabilities appear much sooner in 3DSSF. The transverse cuts in Figure 7 also show the earlier appearance of transverse perturbations and three-dimensionalization in 3DSSF. The small-scale structures are much more prominent in the reattachment region for 3DSM. This is consistent with the higher turbulent intensities obtained with this model in the reattachment and recovery regions and the much lower subgrid-scale dissipation of the model.

Figure 8 shows the instantaneous streamwise vorticity field in a plane close to the surface of the plate. 3DSM exhibits less "coherence" and contains smaller structures with roughly equal characteristic sizes in the spanwise and streamwise directions. The structures become gradually more elongated only after reattachment. Both 3DSF and 3DSSF present a much higher degree of coherence. In 3DSSF structures with streamwise lengths in the range $1d$-$3d$ are apparent. Significant spanwise vorticity levels are not observed till well downstream of separation with the beginning of the break up of the spanwise.

Overall, the selective structure function simulation (3DSSF) produces separated shear layer instabilities, dynamical patterns, and structures which are physically consistent with the flow visualization of Saathoff and Melbourne (1997). Further analysis is therefore confined to this simulation.

Signal Analysis: 3DSSF Simulation

Figure 9a shows the trace of the instantaneous vertical velocity recorded just downstream of separation and within the shear layer. The power density spectrum of this signal is shown in Fig. 9b. Consistent with experimental spectra (Djilali and Gartshore, 1991a), high frequency motion is dominant in the vicinity of separation, and eddies with time scales as small $0.3d/U$ are

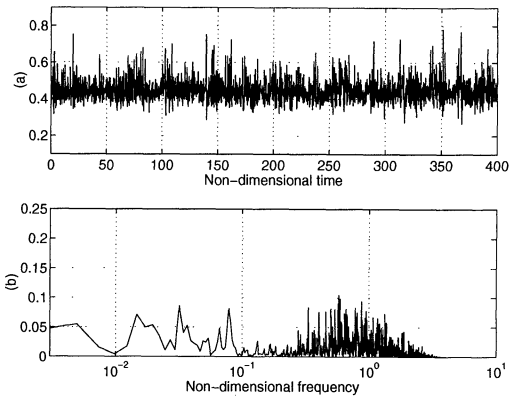

Figure 9: 3DSSF simulation (a) vertical velocity signal at x = $0.493d$, y = $0.47d$, mid-span; (b) power spectrum density

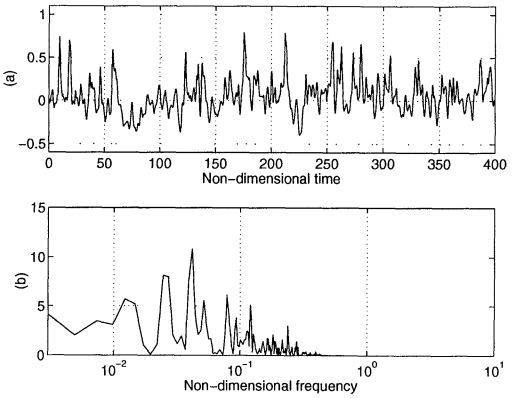

Figure 10: 3DSSF simulation (a) near-wall streamwise velocity signal at x = $4.51d$, mid-span; (b) power spectrum density

deduced. In addition to the high frequency activity centered around $\sim 0.8U/d$, the signal also exhibits peaks in the low frequency range $0.02 \sim 0.08U/d$. This low frequency motion is associated with the so-called flapping of the shear-layer (Kiya and Sasaki; 1983).

To provide further insight into the dynamics of the flow, a time domain analysis using the wavelet transform (see, e.g., Farge, 1992) of the signal near reattachment was conducted. Wavelet analysis has the advantage of providing, simultaneously, information about dominant frequencies/scales *and* their localization in time. Figure 10 shows the streamwise velocity signal at a location close to mean reattachment and the corresponding (Fourier) power spectrum density. Compared to the signal sampled near separation (Fig. 9), there is little energy in the high frequencies. Most of the energy is in the larger scales corresponding to frequencies well below $0.2U/d$. Figure 11 shows the wavelet map of this signal, in terms of relief contours of the absolute value of the wavelet coefficient. The intermittent nature of the large-

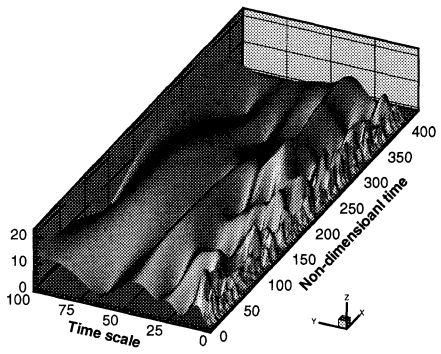

Figure 11: Morlet wavelet map of near-wall velocity signal at x = $4.51d$, mid-span

scale unsteadiness is illustrated along the most distinct range of scales: 20-50d/U. This range corresponds to frequencies of 0.02-0.05U/d and is associated with the low frequency flapping of the shear layer discussed earlier. The intermittency of this phenomenon is clearly shown by the alternating peaks and troughs between 45 and 395 time units. The scales containing the most energy are in the range 5-15d/U, or frequencies of 0.066-0.2U/d. This coincides with the range of frequencies reported experimentally for the pseudo-periodic vortex shedding around reattachment (Cherry *et al.*, 1983; Djilali and Gartshore, 1991a). The localization of these events shows events of relatively short duration, followed by longer quiescent periods. Furthermore, the signal in Figure 10a shows positive fluctuations about the mean which are of a much higher amplitude than the negative fluctuations. This feature and the patterns shown in the wavelet map suggest that a typical cycle consists of two distinct phases: (i) gradual growth of large-scale structures in the separated shear layer, accompanied by a progressive growth of the separation bubble; (ii) shedding of a large scale structure followed by a "collapse" of the bubble and abrupt shortening of the reattachment length.

CONCLUDING REMARKS

Large-eddy simulations of the high Reynolds number ($Re_d = 50,000$) separated-reattaching flow over a bluff plate have been performed with three subgrid-scale models. The mean flow and turbulence statistics obtained with the selective-structure function model provide very good agreement with the pulsed-wire experimental data obtained at the same Reynolds number and blockage ratio in low free-stream turbulence. Although the Smagorinky model yields a reattachment length in good agreement with experiments, the turbulence statistics and dynamics of the flow are deficient. Both this model and the structure function model delay the breakup and three-dimensionalization of the separated shear layer. Farther downstream, where turbulent transport is largely dominated by large scale unsteadiness, the Smagorinky model subgrid-scale dissipation is insufficient, allowing the persistence of small scale turbulent motion, whereas the structure-function model is too dissipative. The localization achieved with the selective structure function model yields lower time-averaged subgrid-scale dissipation and results in dynamic features of separation and reattachment which compare well with flow visualization. The characteristic frequencies and intermittent nature of the pseudo-periodic vortex shedding, as well as the shear layer flapping were captured in the simulations.

ACKNOWLEDGEMENT

The financial support of the Natural Sciences and Engineering Council of Canada (NSERC) is gratefully acknowledged.

REFERENCES

Cherry N.J., Hillier R., and Latour M.E.M.P., 1983, "The unsteady structure of two-dimensional separated and reattaching flows", *J. Wind Eng. & Ind. Aero.*, Vol. 11, pp. 95-105.

Djilali N., and Gartshore I.S., 1991a, "Turbulent flow around a bluff rectangular plate. Part I: Experimental investigation", ASME *J. Fluids Eng.*, Vol. 113, pp. 51-59.

Djilali N., and Gartshore I.S., 1991b, "Turbulent flow around a bluff rectangular plate. Part II: Numerical Predictions", ASME *J. Fluids Eng.*, Vol. 113, pp. 60-67.

Farge M., 1992, " Wavelet transform and their application to turbulence", *Ann. Rev. Fluid Mechanics*, Vol. 24, pp. 395-457.

Ferziger J.H., 1993, "Subgrid scale modeling", Large eddy simulation of complex engineering and geophysical flows, B. Galerpin and S.A. Orzag ed., CUP.

Hillier R., and Cheery N.J., 1981, "The effect of stream turbulence on separation bubble", *J. Wind Eng. & Ind. Aero.*, Vol. 8, pp. 49-58.

Kiya M., and Sasaki K., 1983, "Structure of a turbulent separation bubble", *J. Fluid Mech.*, Vol. 137, pp. 83-113.

Kogaki T., Koyayashi T., and Taniguchi N., 1997, "Large eddy simulation of flow around a rectangular cylinder", *Fluid Dynamics Res.*, Vol. 20, pp. 11-24.

Lane J.C, and Loehrke R.I., 1980, " Leading edge separation from a blunt plate at low reynolds number", ASME *J. Fluids Eng.*, Vol. 102, pp. 494-496.

Le, H., Moin, P. and Kim, J., 1998, "Direct numerical simulation of turbulent flow over a backward facing step", *J. Fluid Mech.*, Vol. 330, pp. 349-374.

Lesieur M., and Métais O., 1996, "New trends in large-eddy simulations of turbulence", *Ann. Rev. Fluid Mechanics*, Vol. 28, pp. 45-82.

Saathoff P.J., and Melbourne W.H., 1997, "Effects of free stream turbulence on surface pressure fluctuations in a separation bubble", *J. Fluid Mech.*, Vol. 337, pp. 1-24.

Suksangpanomrung A., Moinat P., and Djilali N., 1997, "Large-eddy simulation of flow over abluff plate", *Proc. CFD97*, Victoria, pp. 255-262.

Tafti D.K., and Vanka S.P., 1991, "A three dimensional numerical study of flow separation and reattachment", *Phys. Fluids*, A3(12), pp. 2887-2909.